

1  
2  
3  
4  
5  
6  
7  
8  
9  
10  
11  
12  
13  
14  
15  
16  
17  
18  
19  
20  
21  
22  
23  
24  
25  
26  
27  
28

Stokes Drift of Plankton in Linear Internal Waves: Cross-Shore Transport of Neutrally  
Buoyant and Depth-Keeping Organisms

Peter J.S. Franks<sup>1</sup>, Jessica C. Garwood<sup>1</sup>, Michael Ouimet<sup>2</sup>, Jorge Cortes<sup>3</sup>, Ruth C.  
Musgrave<sup>4</sup>, and Andrew J. Lucas<sup>1,3</sup>

<sup>1</sup>Scripps Institution of Oceanography, UCSD, La Jolla CA, 92093

<sup>2</sup>Naval Information Warfare Center Pacific, San Diego CA, 92152

<sup>3</sup>Department of Mechanical and Aerospace Engineering, UCSD, La Jolla CA, 92093

<sup>4</sup>Department of Oceanography, Dalhousie University, Halifax, NS, B3H 4R2

Corresponding author:

Peter J.S. Franks [pfranks@ucsd.edu](mailto:pfranks@ucsd.edu)

Other Authors:

Jessica C. Garwood [jgarwood@ucsd.edu](mailto:jgarwood@ucsd.edu)

Michael Ouimet [Michael.ouimet@navy.mil](mailto:Michael.ouimet@navy.mil)

Jorge Cortes [cortes@ucsd.edu](mailto:cortes@ucsd.edu)

Ruth Musgrave [rmusgrave@dal.ca](mailto:rmusgrave@dal.ca)

Andrew J. Lucas [ajlucas@ucsd.edu](mailto:ajlucas@ucsd.edu)

Keywords: Stokes drift, internal wave, plankton transport, larval transport, meroplankton,  
cross-shore transport

Running head: Stokes drift in internal waves

29 **Abstract**

30 The meroplanktonic larvae of many invertebrate and vertebrate species rely on physical  
31 transport to move them across the shelf to their adult habitats. One potential mechanism  
32 for cross-shore larval transport is Stokes drift in internal waves. Here we develop theory  
33 to quantify the Stokes velocities of neutrally buoyant and depth-keeping organisms in  
34 linear internal waves in shallow water. We apply the analyses to theoretical and measured  
35 internal wave fields, and compare results with a numerical model. Near the surface and  
36 bottom boundaries, both neutrally buoyant and depth-keeping organisms were transported  
37 in the direction of the wave's phase propagation. However, neutrally buoyant organisms  
38 were transported in the opposite direction of the wave's phase at mid depths, while depth-  
39 keeping organisms had zero net transport there. Weakly depth-keeping organisms had  
40 Stokes drifts between the perfectly depth-keeping and neutrally buoyant organisms. For  
41 reasonable wave amplitudes and phase speeds, organisms would experience horizontal  
42 Stokes speeds of several centimeters per second – or a few kilometers per day in a  
43 constant wave field. With onshore-polarized internal waves, Stokes drift in internal  
44 waves presents a predictable mechanism for onshore transport of meroplanktonic larvae  
45 and other organisms near the surface, and offshore transport at mid depths.

46

47

48 **Introduction**

49 Fluctuations of coastal invertebrate and vertebrate populations are often driven by the  
50 supply of larvae to the adult habitat (Gaines and Roughgarden 1985). Many  
51 commercially and ecologically important species have planktonic larval stages, and these  
52 larvae are moved across the shelf at the whim of horizontal currents. Physical transport  
53 may be a key process connecting offshore larval populations with near-coastal settlement  
54 locations, thereby influencing adult populations (e.g., Pineda 1999, Shanks 1983, 2009,  
55 Shanks et al. 2000, Shanks and Brink 2005). Investigation of the physical dynamics of  
56 cross-shore transport is therefore an essential element in understanding fluctuations of  
57 coastal populations with meroplanktonic larvae.

58  
59 Numerous studies have associated the cross-shelf transport of both phytoplankton (e.g.,  
60 Omand et al. 2011) and meroplanktonic larvae (Shanks 1983, Shanks and Wright 1987,  
61 Pineda 1999, Shanks et al. 2014) with internal waves. Theoretical studies suggest that  
62 transport in internal waves would be enhanced with certain swimming behaviors such as  
63 depth-keeping or floating (Lamb 1997, Scotti and Pineda 2007). Moreover, such  
64 behaviors are predicted to lead to accumulation of surface plankton in internal wave  
65 troughs (Franks 1997, Lennert-Cody and Franks 1999, Jaffe et al. 2017).

66  
67 The idea of plankton being transported across the shelf by internal waves associated with  
68 the internal tide has a long history. Kamykowski (1974) was one of the first to model the  
69 transport of swimming plankton in an internal tide, showing that over a tidal cycle,  
70 organisms could be displaced by a kilometer or more. Shanks (1983) tracked Styrofoam  
71 cups weighted with sand as they were transported (or not) in surface slicks formed by  
72 internal waves associated with the internal tide. On some occasions the cups both  
73 accumulated in the slicks, and were transported onshore 1-2 km. Coincident sampling  
74 showed meroplanktonic larvae to have higher concentrations in the slicks than outside the  
75 slicks, suggesting that the internal waves served as a concentrating and transport  
76 mechanism for the larvae.

77

78 Pineda (1999) used a combination of moorings and small-boat sampling in La Jolla Cove,  
79 California, to show that several types of meroplanktonic larvae were concentrated in the  
80 nonlinear waves associated with the internal tide; interestingly, other meroplanktonic  
81 larvae were not concentrated. The data collected supported the inference that the  
82 meroplanktonic larvae – particularly those swimming upward – were transported onshore  
83 in the nonlinear waves, providing a temporally discrete (internal tide period) mechanism  
84 driving local pulses of recruitment. More recently Shanks et al. (2014) concluded from  
85 correlation analyses that barnacle larvae at Carmel River State Beach, CA, were  
86 transported onshore by internal tides.

87

88 Lamb (1997) was one of the first to calculate theoretical transport distances of surface-  
89 trapped plankton in solitary nonlinear waves. He showed that displacement varied  
90 nonlinearly with the wave's maximum horizontal velocity; net displacements of a few  
91 hundred meters were expected for wave phase speeds of  $\sim 0.25 \text{ m s}^{-1}$ , while maximum  
92 displacements  $>3 \text{ km}$  were predicted for phase speeds  $>0.5 \text{ m s}^{-1}$ . Scotti and Pineda  
93 (2007) showed that organisms with stronger depth-keeping abilities could travel greater  
94 distances in nonlinear fronts than weaker depth-keeping organisms.

95

96 Curiously, in spite of the considerable body of work exploring planktonic transport in  
97 linear and nonlinear internal waves, little attention has been paid to investigating  
98 transport of plankton by the Stokes velocity driven by the linear internal wave field.  
99 Stokes velocity is the velocity following a fluid parcel as it moves with the wave-induced  
100 velocities, averaged over a wave period. It arises from the difference between the average  
101 Lagrangian velocity of the parcel, and the average Eulerian velocity at a fixed location  
102 (summarized nicely in Craik 2005). Stokes drift has been well described for surface  
103 waves, in which a fluid parcel moves in the direction of the wave's phase propagation,  
104 with its horizontal displacement depending on depth below the free surface. Previous  
105 work has explored the Stokes velocities driven by linear internal waves over a sloping  
106 bottom (Wunsch, 1971), and in lakes (Henderson, 2016). These papers support our results  
107 (below) that for a linear internal wave in a stratified fluid, the magnitude, and in  
108 particular the direction of the Stokes velocity, depend on the stratification. In the present

109 analysis we show in addition that the Stokes velocity experienced by an organism  
110 depends on the organism's behavior.  
111  
112 Near a boundary, any onshore Stokes flow must be balanced by an offshore Eulerian  
113 mean flow or vertical mixing, in order to satisfy continuity (e.g., Wunsch, 1971; Ou and  
114 Maas, 1986). Where the Eulerian mean flow cancels the Stokes drift, passive organisms  
115 would not experience any net horizontal transport. Organisms that can move relative to  
116 the water, however, can escape this constraint, and experience net cross-shore  
117 displacements in periodic waves, as discussed below. However, with mixing,  
118 intermittency of the internal waves, and set-up time, the Eulerian mean flow may not  
119 exactly balance the Stokes drift at any given time and location. Thus, internal waves have  
120 the potential to persistently transport swimming plankton onshore, even though long-term  
121 average mass or momentum balances limit net water transport.

122  
123 Here we consider two extremes of organism behavior: neutrally buoyant and depth-  
124 keeping. Neutrally buoyant organisms follow the water parcels perfectly, while depth-  
125 keeping organisms maintain a particular depth (pressure) surface, swimming perfectly  
126 against any vertical currents. We will show below that weaker swimmers experience  
127 Stokes drifts somewhere between passive and depth-keeping organisms, depending on  
128 their maximum swimming speeds. We build on theory presented by Thorpe (1968) for  
129 passive particles in linear internal waves, and a subsequent derivation by Dewar (1980)  
130 who explored the Stokes drift of passive and depth-keeping floats, using the general  
131 equations of Henderson (2016) to derive solutions giving the Stokes velocity for neutrally  
132 buoyant and depth-keeping plankton in linear internal waves with varying stratification.  
133 We derive general expressions for the Stokes velocity, allowing the incorporation of  
134 arbitrary measured profiles of density and vertical velocity (for example, from upward-  
135 looking Acoustic Doppler Current Profilers (ADCPs) or time-series of fluctuations of the  
136 depths of isopycnals). We test our analytical solutions using the MITgcm numerical  
137 model configured to simulate a 2-D (depth, cross-shore distance) section containing  
138 organisms with swimming abilities ranging from fully passive (neutrally buoyant) to  
139 perfectly depth-keeping, being moved by linear internal waves. We show that for

140 reasonable wave amplitudes and phase speeds, the cross-shore Stokes velocity is a few  
141 centimeters per second – or a few kilometers per day in a constant wave field. However,  
142 it is the depth-dependence of the direction of the Stokes velocity that is particularly  
143 intriguing, and its dependence on stratification and organism behavior.

144

### 145 **Internal wave stream function**

146 We describe the water motions in continuously stratified, mode-1 linear internal waves  
147 using a stream function  $\psi(x,z,t)$  (e.g., Thorpe 1968, Lennert-Cody and Franks 1999):

148

$$149 \quad \psi(x,z,t) = A_{\max} \frac{\omega}{k} S_w(z) \cos(kx - \omega t). \quad (1)$$

150

151 Here  $A_{\max}$  is the maximum vertical displacement of a water parcel from its equilibrium  
152 depth as the wave passes by (i.e., the wave's maximum amplitude), having dimensions of  
153 length. The vertical dependence of the wave's vertical velocity is given by the structure  
154 function  $S_w(z)$  which is dimensionless, and varies between 0 at the upper and lower  
155 boundaries and 1 at the depth of maximum vertical displacement for a mode-1 wave. The  
156 wave has frequency  $\omega$  and horizontal wavenumber  $k$ , and is periodic in the horizontal  
157 direction. The wave's phase speed is  $c = \omega/k$ . Contours of this stream function (1) in  
158  $(x,z,t)$  give the paths of water parcels – and neutrally buoyant organisms – as the wave  
159 propagates.

160

161 The wave's horizontal ( $u(x,z,t)$ ) and vertical ( $w(x,z,t)$ ) velocities can be found from the  
162 stream function (1) as:

163

$$164 \quad u(x,z,t) = \frac{\partial \psi}{\partial z}, \quad w(x,z,t) = -\frac{\partial \psi}{\partial x}. \quad (2)$$

165

### 166 **Stokes Velocities: General Solutions**

167 Here we calculate general analytical solutions for the Stokes velocities of neutrally  
168 buoyant and depth-keeping organisms in linear internal waves. As we show below, these

169 cases represent two extremes of organism behavior. Neutrally buoyant organisms would  
 170 be wafted around by the ambient currents, not moving relative to the fluid around them.  
 171 Depth-keeping organisms exactly balance the wave’s vertical motions to maintain a  
 172 particular depth in the water column. Though this latter case may not be realistic (c.f.  
 173 Lennert-Cody and Franks 2002), the conditions for most organisms will lie somewhere  
 174 between these two cases, as we show below.

175  
 176 Neutrally buoyant organisms are assumed to follow the trajectories of water parcels, both  
 177 vertically and horizontally. To find the general form of the Stokes velocity for neutrally  
 178 buoyant organisms in the internal wave (Eq. 1) we follow Thorpe (1968) and others in  
 179 defining  $x = x_0 + x_1$  and  $z = z_0 + z_1$ , where  $(x_0, z_0)$  is assumed to be independent of  $t$ , and  
 180  $(x_1, z_1)$  is small in magnitude. Noting that, in the absence of any non-wave-driven  
 181 Eulerian mean flow, and taking only leading-order wave fluctuations,

$$\begin{aligned}
 \frac{dx_1}{dt} &= u = \frac{\partial \psi}{\partial z} \\
 \frac{dz_1}{dt} &= w = -\frac{\partial \psi}{\partial x}
 \end{aligned}
 \tag{3}$$

184  
 185 the Stokes velocity is given by (e.g., Henderson, 2016)

$$u_{Snb} = \langle x_1 \frac{\partial u}{\partial x} \rangle + \langle z_1 \frac{\partial u}{\partial z} \rangle,
 \tag{4}$$

188  
 189 where the subscript “*Snb*” denotes “Stokes, neutrally buoyant”, and the angle brackets  
 190 indicate an average over a wave period:

$$\langle \cdot \rangle = \frac{\omega}{2\pi} \int_0^{\frac{2\pi}{\omega}} \cdot dt.
 \tag{5}$$

193  
 194 The first term on the right-hand side of (4) gives the horizontal movement of a neutrally  
 195 buoyant organism driven by horizontal gradients of the horizontal velocity – the  
 196 horizontal strain,  $\partial u / \partial x$ . This horizontal strain generates regions of convergence and

197 divergence that propagate with the wave. The second term on the right-hand side of (4)  
 198 gives the depth-dependency of the horizontal displacement of an organism. Here, the  
 199 vertical shear of the horizontal velocity,  $\partial u/\partial z$ , drives varying horizontal displacements  
 200 with depth. For weakly nonlinear waves, we can evaluate (4) at leading order by noting  
 201

$$\begin{aligned}
 202 \quad x_1 &= \int u dt \\
 203 \quad z_1 &= \int w dt
 \end{aligned} \tag{6}$$

204  
 205 and calculating  $u$  and  $w$  from (2) and (3). Substituting those into (4) and averaging over a  
 206 wave period  $2\pi/\omega$  we obtain

$$207 \quad u_{Snb} = \frac{A_{max}^2 \omega}{2k} \left[ \left( \frac{\partial S_w(z)}{\partial z} \right)^2 + S_w \frac{\partial^2 S_w(z)}{\partial z^2} \right]. \tag{7}$$

209  
 210 This is the general formulation for the second-order horizontal Stokes velocity for a  
 211 neutrally buoyant organism in a linear internal wave described by (2) (Thorpe, 1968).  
 212

213 The horizontal Stokes velocity for a depth-keeping organism,  $u_{Sd-k}$  (where the subscript  
 214 “ $Sd-k$ ” denotes “Stokes, depth-keeping”) can be found from (4) by noting that a depth-  
 215 keeping organism will not experience any vertical displacement. Thus  $z_1=0$ , and the  
 216 second term on the right-hand side of (4) is zero. This gives

$$217 \quad u_{Sd-k} = \left\langle x_1 \frac{\partial u}{\partial x} \right\rangle \tag{8}$$

219  
 220 and, with substitution of (2), (3), and (6),  
 221

$$222 \quad u_{Sd-k} = \frac{A_{max}^2 \omega}{2k} \left( \frac{\partial S_w(z)}{\partial z} \right)^2. \tag{9}$$

223  
 224 This gives the second-order Stokes velocity of a depth-keeping organism in the internal  
 225 wave described by (2).



226

### 227 **Vertical Structure of the Internal Wave: $S_w(z)$**

228 We will consider three wave forms derived from different vertical density profiles: linear,  
229 pycnocline, and measured.

230

#### 231 *Linear density profile*

232 For a mode-1 wave, a linear density profile gives the structure function (Thorpe 1968):

233

$$234 \quad S_w(z) = \sin \frac{\pi z}{H} \quad (10)$$

235

236 where  $H$  is the water depth (Fig. 1a-c).

237

#### 238 *Pycnocline density profile*

239 We can produce an analytical density profile  $\rho(z)$  with a pycnocline using the hyperbolic  
240 tangent function:

241

$$242 \quad \rho(z) = \rho_o \left[ 1 + \Delta\rho \tanh \left( \frac{z - z_{pyc}}{z_{scale}} \right) \right] \quad (11)$$

243

244 where  $\rho_o$  is a reference density,  $\Delta\rho$  is the density difference from the surface to the  
245 bottom,  $z_{pyc}$  is the depth of the pycnocline, and  $z_{scale}$  scales the vertical thickness of the  
246 pycnocline and thus the local density gradient. Using this density profile gives a structure  
247 function for the mode-1 internal wave (Thorpe 1968) (Fig. 1e-g)

248

$$249 \quad S_w(z) = sech^{kz_{scale}} \left( \frac{z - z_{pyc}}{z_{scale}} \right). \quad (12)$$

250

#### 251 *Measured velocity profile*

252 Field measurements for  $S_w(z)$  were obtained offshore of the Scripps Pier in San Diego,  
253 CA. A Teledyne Sentinel V 5-beam acoustic Doppler current profiler (ADCP) was

254 mounted on the bottom in ~18 m of water, recording velocities at 2 Hz over 21 d.  
255 Vertical profiles of temperature were obtained from RBRsolo temperature loggers placed  
256 with 1 m separation on a mooring, and sampling at 2 Hz. In this region, temperature is the  
257 dominant determinant of vertical density variations, with salinity playing a very minor  
258 role (e.g., Lucas et al., 2011).

259

260 Between the near-surface and 2 m above the bottom, 26 0.6-m-thick depth bins were used  
261 to evaluate the vertical structure of the vertical velocity over 12.42 hour time periods (one  
262 M2 tidal period). Three tidal periods with differing vertical stratification were chosen for  
263 analysis. The vertical velocities, measured by the vertical-looking fifth beam of the  
264 ADCP, were averaged over 30 s intervals and decomposed using empirical orthogonal  
265 functions (EOFs). The first EOF of vertical velocity typically represents the vertical  
266 velocity structure of the mode-1 waves, particularly when the barotropic signal is weak.  
267 The mode-1 vertical velocity (the first EOF) explained 30-57% of the variance in the  
268 measured vertical velocity. For our analyses, we chose time periods when the first EOFs  
269 represented the structure of mode-1 waves. This EOF was scaled to have values between  
270 0 and 1, and was used as the estimate of the vertical structure function  $S_w(z)$  for the  
271 measured wave field.

272

273 In order to estimate  $S_w(z)$ , the values of the first EOF of vertical velocity were fit with a  
274 5<sup>th</sup> order polynomial, and interpolated and extrapolated to depths from the shallowest bin  
275 resolved (1.75 m) to the bottom (18 m) with 0.25 m resolution using the boundary  
276 condition  $S_w(z) = 0$  at  $z = 0$  m and  $z = 16.25$  m. The polynomial was then differentiated to  
277 obtain  $dS_w(z)/dz$  and  $d^2S_w(z)/dz^2$  for calculating the Stokes velocities (7) and (9).

278

### 279 *Numerical Model*

280 To support the analytical analyses and field data, we configured the MITgcm to explore  
281 Stokes drift of particles with behaviors ranging from neutrally buoyant to depth-keeping  
282 in a linear internal wave field. The internal wave flow field was generated in a 2D model  
283 domain with a 50.5 m deep water column that covered 2 km in the horizontal direction.  
284 The grid resolution was 0.5 m in the vertical and 0.3 m in the horizontal. The left and

285 right domain boundaries were open, each with a sponge layer. A free-slip condition was  
286 imposed at the bottom boundary, and the surface was free. Note that the actual water  
287 depth is relatively unimportant in these models, as the depth-dependence of the Stokes  
288 velocities does not depend on the thickness of the water column, just the shape of  $S_w(z)$   
289 (1, 7 and 9).

290

291 Internal waves were generated within part of the domain by nudging density toward the  
292 linear solution for a rightward-propagating mode-1 wave with no rotation:

293

$$294 \quad \frac{d^2 S_w(z)}{dz^2} + \frac{N^2(z) - \omega^2}{\omega^2} S_w(z) = 0 \quad (13)$$

295 The region of internal wave generation spanned two wavelengths in width and covered  
296 the entire water column, immediately to the right of the left-hand sponge layer. To the  
297 right (onshore) of this region, waves propagated freely. In the model, the buoyancy  
298 frequency  $N(z)$  was set to be constant with depth (linear stratification), the non-  
299 hydrostatic properties of the model were turned off, and the Coriolis parameter  $f$  was set  
300 to zero (no rotation). Motivated by the data (below), internal waves at a 25-minute  
301 forcing period ( $\omega \approx 4.2 \times 10^{-3}$  rad/s) were generated in stratifications of  $N \approx 8.7 \times 10^{-3}$  rad/s,  
302 which corresponds to a temperature difference of  $\sim 2$  °C over 50 m depth. Because of the  
303 linear stratification and small wave amplitude, the wave elevations that were generated  
304 were sinusoidal horizontally. The model was configured with a 1 s time step, and the  
305 flow field was saved every 20 s.

306

307 Columns of depth-keeping and passive particles were seeded offline, every 0.5 meter in  
308 the vertical, eight wavelengths away from the wave generation region, and advected  
309 using linear interpolations of the flow field output. Horizontal displacements averaged  
310 over one wave period were used to calculate Stokes velocities; wave properties were  
311 extracted for comparison with the general solutions presented below. Particles with  
312 variable maximum swimming speeds, expressed as a fraction of the maximum wave  
313 vertical velocities, were included to further explore the effects of swimming behavior on  
314 Stokes drift. Swimming particles were coded to have the same target depth as the depth-

315 keeping particles; they opposed displacing vertical currents exactly until the vertical  
316 currents exceeded their maximum swimming speed, at which point they swam at their  
317 maximum speed.

318

## 319 **Results and Discussion**

320 Using (7) and (9), and the theoretical (10, 12) or measured  $S_w(z)$  we can now calculate the  
321 horizontal Stokes velocities of neutrally buoyant and depth-keeping plankton in a variety  
322 of continuously stratified mode-1 linear internal waves (Table 1). The drift patterns of  
323 neutrally buoyant and depth-keeping organisms show some similarities, and some  
324 perhaps surprising differences (Fig. 1d, h). In general, the Stokes velocity for both types  
325 of organism is low in regions where the stratification is low, or more specifically, where  
326 the vertical gradient of  $S_w(z)$  is small. The Stokes velocity also tends to be similar for the  
327 two organism behaviors near the boundaries, where  $S_w(z)$  goes to zero. The presence of a  
328 boundary at the surface and the bottom ensures that there are no vertical internal-wave-  
329 driven velocities there, and vertical swimming is inhibited by the boundary. Thus, by  
330 continuity, the horizontal Stokes velocities are often strongest in these regions, though  
331 this depends on the shape of  $S_w(z)$ .

332

333 Because deep-water linear internal waves can become nonlinear in shallow water, the  
334 waves simulated using the MITgcm needed to have small amplitudes to remain linear; the  
335 waves selected showed a maximum amplitude (isotherm displacement) of 0.6 m, a  
336 wavelength of 210 m, and a maximum vertical velocity of  $2.7 \times 10^{-3} \text{ m s}^{-1}$ . These values  
337 were used in conjunction with the structure of the waves' vertical velocities  $S_w(z)$  (linear  
338 stratification, Fig. 1b) to calculate analytical predictions of Stokes velocities. Agreement  
339 between model results and analytical predictions (7, 9) is nearly perfect (Fig. 2), with  
340 small differences near the boundary, likely due to the offline interpolation scheme and the  
341 approximations made to derive (7) and (9).

342

343 The field data provide an example of realistic wave properties; they show that the  
344 measured maximum vertical velocities (the amplitudes of the first EOF at each time  
345 point) were normally distributed with a mean of -0.89 cm/s and a standard deviation of

346 4.54 cm/s over the course of the 21-day deployment. A power spectrum of the first EOF  
347 vertical velocities was calculated as the average of nine 1024-point (512 min) sections  
348 from nine separate 12.42 h data periods. The power spectrum had a pronounced high-  
349 frequency internal wave peak with 20 to 30 min periods (Fig. 3). To calculate  
350 approximate Stokes velocities from the observations we assumed a wave with a 25 min  
351 period, a 200 m horizontal wavelength, and amplitude of 2 m (Fig. 4). The 2 m amplitude  
352 was chosen to ensure that the modeled waves were linear (i.e.,  $A_{max} \approx 10\%$  of the water  
353 depth).

354

355 The main difference between the Stokes velocities of neutrally buoyant and depth-  
356 keeping organisms is that depth-keeping organisms always move in the direction of the  
357 wave's phase propagation, whereas neutrally buoyant organisms can move either with the  
358 wave, or in the opposite direction of the wave, depending on the organism's depth in  
359 relation to the structure of  $S_w(z)$ . This is particularly apparent at mid-depths, where  
360 neutrally buoyant organisms will drift in the opposite direction of the internal wave,  
361 while depth-keeping organisms will oscillate around their mean position. Integrating (7)  
362 from the surface ( $z=0$ ) to the bottom ( $z=H$ ) with boundary conditions  $S_w(0) = S_w(H) = 0$   
363 shows that the vertically integrated Stokes drift of neutrally buoyant organisms is zero. It  
364 is difficult to perform a similar integration of (9), though it is clear that there is a  
365 vertically integrated net flux of depth-keeping organisms in the direction of the wave's  
366 phase.

367

### 368 *Neutrally buoyant organisms*

369 The general form for the Stokes velocity of neutrally buoyant organisms is given by (4),  
370 and for this stream function (1) by (7) (Table 1). Near the boundaries, neutrally buoyant  
371 organisms will drift in the direction of the wave's phase propagation. At the depth of the  
372 maximum vertical velocity (usually the mean pycnocline depth), however, such  
373 organisms will travel in the *opposite* direction of the wave's phase (Figs. 1d, h). This  
374 conclusion is consistent with other author's analyses (e.g., Wunsch, 1971; Henderson,  
375 2016). Near the coast, internal waves tend to be refracted to propagate onshore-offshore,  
376 with offshore-directed waves originating mainly from reflected onshore waves that did

377 not lose their energy to mixing. Furthermore, even waves propagating obliquely to the  
378 coast will have a cross-shore component to the Stokes drift. Given this predominant  
379 onshore polarization of the internal wave field, the pycnocline presents a pathway for  
380 predictable *offshore* transport of neutrally buoyant organisms, while the near-surface and  
381 near-bottom layers are regions of predictable *onshore* transport (Fig. 1d, h).

382

383 In the measured wave fields, the predicted Stokes velocity for neutrally buoyant  
384 organisms was strongly onshore (in the direction of the wave's phase propagation) in the  
385 upper few meters (above the pycnocline), offshore between ~10-14 m above bottom, and  
386 very weakly onshore below (Fig. 4c, f, i), consistent with the vertical structure of the  
387 theoretical density distributions above (10 and 12) (Fig. 1d, h). Because of the vertical  
388 asymmetry of the observed vertical velocity structure function  $S_w(z)$ , the Stokes velocities  
389 were much stronger in the surface waters (onshore), and at the pycnocline (offshore),  
390 than the rest of the water column below.

391

392 Stokes velocities predicted from the data were a few cm/s through most of the water  
393 column, but reached up to 5 cm/s near the surface. These large surface values should be  
394 viewed with some skepticism, as the EOF of vertical velocity is not well defined in this  
395 region due to limitations of the ADCP. Though small, these horizontal drift speeds would  
396 result in cross-shore displacements of several kilometers per day.

397

### 398 *Depth-keeping organisms*

399 The Stokes velocity of depth-keeping organisms is given by (9) (Table 1). The  
400 fundamental difference between the drifts of depth-keeping and neutrally buoyant  
401 organisms is that depth-keeping organisms always drift in the direction of the wave  
402 propagation throughout the water column. The Stokes velocity of depth-keeping  
403 organisms is zero at the depth of the maximum vertical velocity (where  $dS_w(z)/dz = 0$ ),  
404 with peak drift speeds displaced above and below the vertical velocity maximum (Figs.  
405 1d, h and 4c, f, i). At these mid depths, where neutrally buoyant organisms have a  
406 maximum offshore Stokes velocity, the depth-keeping behavior counteracts the offshore  
407 Stokes drift, keeping the organisms relatively stationary (horizontally and vertically) over

408 a wave period. At the surface and bottom boundaries the Stokes velocities for neutrally  
409 buoyant and depth-keeping organisms are the same: in this region the internal-wave  
410 vertical velocities are small compared to the horizontal velocities that drive the Stokes  
411 drift, making it a more one-dimensional (horizontal) system in which organisms always  
412 drift in the direction of the wave's phase propagation.

413

414 The inferred Stokes velocities for depth-keeping organisms in the measured velocity field  
415 (Fig. 4c, f, i) were strongly in the direction of the wave's phase in the upper few meters,  
416 and weak through the rest of the water column. The predicted strong near-surface drift  
417 speeds (up to 5 cm/s) were partly a consequence of the limited spatial sampling range of  
418 the ADCP, which presents problems in measuring velocities near the surface and bottom  
419 boundaries. However, these strong surface drift speeds are also a consequence of the  
420 steep gradients of  $S_w(z)$  in the upper water column relative to the deeper water column.  
421 This asymmetry is not obviously related to the stratification, and seemed to persist in  
422 both weakly and strongly stratified conditions (Fig. 4). No matter the source of the  
423 asymmetry, the consequence was that organisms within 3-5 m of the surface – regardless  
424 of their swimming behavior – would experience much stronger Stokes drift speeds in the  
425 direction of wave propagation than organisms in the rest of the water column.

426

#### 427 *Dependence on wave properties*

428 The theoretical calculations predict that, for a given frequency and amplitude, a stronger  
429 pycnocline can support larger vertical velocities of an internal wave, and these increased  
430 vertical velocities will generate stronger Stokes velocities. Stokes velocities are directly  
431 proportional to the wave's phase speed  $\omega/k$ , and increase as the square of the wave  
432 amplitude for both depth-keeping and neutrally buoyant organisms (7) and (9).

433

434 The dependence of the Stokes velocity on the density structure of the water column is not  
435 obvious from equations (7) and (9). It is clear that stronger vertical gradients of the  
436 vertical velocity (large  $dS_w(z)/dz$ ) will tend to generate stronger speeds for depth-keeping  
437 organisms. However, the Stokes velocity for neutrally buoyant organisms depends  
438 additionally on the local curvature of  $S_w(z)$ .

439

440 *Weakly depth-keeping organisms*

441 That neutral buoyancy and depth-keeping are two ends of a continuum of swimming  
442 strategies is well demonstrated by the numerical model results (Fig. 5). Here, weakly  
443 depth-keeping organisms were programmed to counteract the vertical velocities until the  
444 wave-driven vertical velocities were stronger than the organism's maximum swimming  
445 speed. At this point the Stokes velocities of the organisms tend toward those of neutrally  
446 buoyant organisms. The lower the organism's maximum vertical swimming speed, the  
447 more closely its Stokes velocity profile resembled that of a neutrally buoyant organism  
448 (Fig. 5). This is most noticeable in the mid water column where the wave's vertical  
449 velocities are highest.

450

451 *Swimming strategies for transport*

452 As demonstrated above, neutrally buoyant and depth keeping represent end-members of a  
453 spectrum of a plankter's ability to swim against ambient vertical velocities (Fig. 5). The  
454 local magnitude of  $S_w(z)$  is proportional to the local standard deviation of the vertical  
455 velocity: a wave's vertical velocities are maximum at mid depths, and decay to zero at the  
456 boundaries (Fig. 1b, f). This implies that depth-keeping plankton require increasingly  
457 greater swimming abilities as they approach mid depths to be able to oppose the wave  
458 velocities and maintain depth.

459

460 At the surface and bottom boundaries, vertical currents are negligible, and by continuity  
461 the horizontal currents the strongest. Here the neutrally buoyant, weakly depth-keeping,  
462 and fully depth-keeping organisms' Stokes velocities all converge: they are maximal, and  
463 aligned with the phase propagation of the wave, driving a predictable transport of  
464 organisms. Near the coast, the onshore-offshore polarization of internal waves would  
465 give a tendency for onshore Stokes velocities near the surface, in the direction of the  
466 wave propagation. Because of the weak vertical wave velocities near the surface, even  
467 weak swimmers such as dinoflagellates or ciliates would be able to exploit this wave-  
468 driven onshore transport (although see Eulerian mean flows below). Meroplanktonic  
469 larvae with large amounts of lipids, such as asteroids, holothurians, and anthozoans, or



470 some nectochaete polychaete larvae with large oil droplets (Chia et al. 1984) will tend to  
471 float. Trapped at the surface, floating organisms are effectively depth keepers, giving  
472 them a predictable mechanism to move them toward their nearshore adult habitat.  
473 Similarly, sinking organisms will tend to be moved onshore close to the bottom.

474

475 In the middle of the water column it will take considerably more effort for an organism to  
476 counteract the internal-wave-driven vertical velocities, which can reach a few centimeters  
477 per second. Neutrally buoyant meroplanktonic larvae will tend to be transported offshore  
478 in onshore-propagating internal waves, giving a predictable pathway for offshore  
479 dispersion of weak-swimming meroplanktonic larvae. Stronger swimmers that can depth-  
480 keep against the internal wave vertical velocities will tend to have little horizontal  
481 displacement near the pycnocline. Such a strategy does not seem to have much practical  
482 benefit, however, given the more predictable cross-shore transports of passive organisms  
483 near the pycnocline (offshore) or surface (onshore).

484

#### 485 *Eulerian mean flows*

486 In theory, if there is a steady Stokes flow of water toward a boundary, at equilibrium an  
487 Eulerian mean return flow should set up that would exactly oppose the Stokes flow (e.g.,  
488 Wunsch 1971). Without mixing, water parcels would flow back along the same  
489 isopycnals; thus, at equilibrium, water parcels or passive organisms would experience no  
490 net transport. In an open channel, the Coriolis effect can produce similar results. This  
491 setup of an Eulerian mean flow was recently observed in situ where internal waves  
492 intersected the slope of a narrow lake (Henderson 2016).

493

494 In this non-mixing context, the net transport experienced by any organism that can move  
495 with respect to water parcels will be given by the sum of the Stokes drift they experience,  
496 and the displacement associated with the Eulerian mean flow at their depths.

497 Interestingly, therefore, in the parts of the water column where passive and depth-keeping  
498 organisms experience similar Stokes drift (i.e., near the boundaries), the Eulerian mean  
499 flow will cancel both the passive and depth-keepers' Stokes drift. However, in mid water  
500 column, depth-keeping organisms experience no Stokes drift. This means that – in this

501 equilibrium, non-mixing situation – the total transport of mid-depth depth keepers will be  
502 exclusively due to the Eulerian mean flow: it will be maximum at this depth, and in the  
503 opposite direction to that predicted by the Stokes drift of passive organisms. Thus, on  
504 average in this equilibrium situation, depth-keeping organisms at mid-depths in the water  
505 column with onshore-propagating waves would be moved toward shore.

506

507 However, it remains unclear whether this theoretical equilibrium situation would occur in  
508 a realistic, time-dependent, mixing, topographically constrained ocean. For instance,  
509 internal waves may dissipate before reaching the seabed, while mixing may prevent  
510 isopycnals from intersecting the slope and/or allow for a return flow that is not along the  
511 original isopycnals. Both these situations would weaken or eliminate the balance between  
512 the local Stokes drift and the Eulerian mean flow. Furthermore, the Eulerian mean flow  
513 sets up at equilibrium; internal waves, however, are often intermittent (e.g., associated  
514 with the internal tide), with changing background stratification and flow conditions  
515 leading to a variable internal-wave climate (Nash et al. 2012). These spatial and temporal  
516 variations in the Stokes flow are not likely to be exactly balanced by the equilibrium  
517 Eulerian flow, allowing organisms to be transported with the Stokes flow generated by  
518 internal waves.

519

520 Given the potential for an Eulerian mean flow opposing the internal-wave-driven Stokes  
521 drift, the Stokes drift predictions presented in this study should be considered in the  
522 larger context of the local mean flows. For instance, recent observations showed that a  
523 swarm of underwater, depth-keeping larval mimics experienced net onshore transport  
524 during the passage of an internal wave interacting with a mean flow (Garwood et al.,  
525 unpubl.). In this context, it is worth noting that the numerical model used in the present  
526 study had no boundaries, so no Eulerian mean flow was set up. The set-up timescale  
527 would be expected to depend on achieving a geostrophic balance through Coriolis, thus  
528 about an inertial period. The question is whether the balancing Eulerian mean flow would  
529 set up within a time scale that would cancel the net transport of larvae: the organisms  
530 might reach their nearshore adult habitat before such an Eulerian mean flow affected  
531 them. The opposing dynamics of the Stokes drift and the opposing Eulerian mean flow

532 need to be more carefully considered in the context of a space- and time-dependent ocean  
533 wave field.

534

#### 535 *Transport in nonlinear waves*

536 Using a 25-minute wave period, the displacements derived from *in situ* profiles of  $S_w$   
537 (Fig. 4) ranged from -44-144 m for passive organisms, and 0-153 m for depth-keeping  
538 organisms over a single wave. The largest displacements were near the surface and  
539 bottom boundaries, and were in the direction of wave propagation. Passive organisms 12-  
540 15 m above the bottom tended to be transported offshore over a wave period. These  
541 results are comparable to estimates of surface transport by nonlinear internal waves on  
542 the New Jersey's shelf (Shroyer et al. 2010), where the first three waves of numerous  
543 wave packets were found to induce surface transports of a few hundred meters. Transport  
544 integrated vertically over the surface layer can be calculated by integrating velocities in  
545 depths shallower than the maximum value of  $S_w(z)$ . Extrapolating Stokes velocities  
546 calculated from our shallowest ADCP bin to the surface, and vertically integrating  
547 velocities over the surface layer yielded transport estimates of 0.007-0.16 m<sup>2</sup>/s for passive  
548 organisms, and 0.03-0.23 m<sup>2</sup>/s for depth-keeping organisms over a wave period. These  
549 values are considerably lower than estimates of 5 m<sup>2</sup>/s during wave events and 0.2-0.5  
550 m<sup>2</sup>/s over the course of a day estimated by Inall et al. (2001), Shroyer et al. (2010), and  
551 Zhang et al. (2015). Although the wave amplitude to water depth ratios were similar in all  
552 studies, the surface layer in our study was much thinner: it extended down to 7 m, on  
553 average, in 18 m of water, compared to 20-50 m in 100-150 m of water for other studies.  
554 The maximum wave-induced velocities and wave propagation speeds associated with our  
555 data-based simulations were of order 0.1 m/s, while those measured for the large,  
556 nonlinear internal waves referenced above were approximately 5 times larger. The ratio  
557 of maximum wave-induced velocities and wave propagation speeds were thus similar.

558

559 Comparing transport observed in internal waves on the Malin shelf with theoretical  
560 predictions, Inall et al. (2001) found the linear terms of a weakly nonlinear solution  
561 accounted for 70% of the observed transport, while nonlinear terms accounted for the  
562 remaining 30%. Though linear solutions generate conservative estimates of transport –

563 especially in shallow waters where internal waves steepen and become highly nonlinear –  
564 Inall et al.’s solutions suggest that linear waves can drive a significant fraction of the total  
565 transport. The linear approximations presented here, however, include organism behavior  
566 in response to the waves, and the fact that organisms travel with the wave; it is often the  
567 case that velocity measurements are integrated over time at a point (e.g., a mooring or  
568 ADCP), without propagating organisms with the flow field. Given that most waves in  
569 relatively shallow waters near the coast are nonlinear to some degree, both our linear  
570 estimates and Eulerian observations are likely to underestimate the actual transport  
571 experienced by organisms. One particularly large, highly nonlinear wave event captured  
572 on the New Jersey shelf was associated with onshore displacements of up to 2 km  
573 (Shroyer et al. 2010). Because larger waves have larger vertical velocities, stronger  
574 swimming abilities would be required to regulate an organism’s depth. In such large  
575 waves, depth-keeping may not be a very effective strategy relative to depth-keeping in  
576 linear or weakly nonlinear internal waves.

577

578

## 579 **Conclusions**

580 We have derived general equations for the Stokes velocities of neutrally buoyant (4, 7)  
581 and depth-keeping (8, 9) organisms in linear internal waves. The vertical structure of the  
582 Stokes velocity depends on the structure function of the vertical velocities,  $S_w(z)$ , which  
583 can be measured in the field with an ADCP (a 5 beam ADCP being especially attractive  
584 for this purpose). Our analyses show that near the surface and bottom, both behaviors  
585 lead to Stokes transports in the direction of the phase propagation of the wave. At mid  
586 depths, however, where vertical velocities are maximal, neutrally buoyant organisms drift  
587 in the opposite direction of the wave’s phase, while depth-keeping organisms are  
588 stationary. Organisms that are weakly depth keeping will have transport speeds and  
589 directions between those of neutrally buoyant and perfectly depth-keeping organisms.  
590 The Stokes velocities increase with the wave’s phase speed and amplitude, generating  
591 speeds of a few centimeters per second or a few kilometers per day. Near the coast, where  
592 internal waves tend to be onshore-offshore polarized, internal-wave-driven Stokes drift

593 presents a predictable cross-shore transport pathway for meroplanktonic larvae to travel  
594 toward or away from coastal adult habitats.

595

596 **Acknowledgements**

597 The authors wish to thank Michael Allshouse for generously providing his RK4 gridded  
598 interpolants routine to generate particle positions more efficiently in the numerical model.

599 This manuscript benefitted greatly from the insightful critiques of two anonymous  
600 reviewers, and we thank them for their time and input. This work was supported by NSF  
601 grant OCE-1459393.

602

603  
604  
605  
606  
607  
608  
609  
610  
611  
612  
613  
614  
615  
616  
617  
618  
619  
620  
621  
622  
623  
624  
625  
626  
627  
628  
629  
630  
631  
632  
633  
634  
635  
636  
637  
638  
639  
640  
641  
642  
643  
644  
645  
646

## References

- Chia, F.-S., Buckland-Nicks, J. & Young, C.M., 1984. Locomotion of marine invertebrate larvae: a review. *Canadian Journal of Zoology*, 62(7), pp.1205–1222.
- Craik, A.D.D., 2005. George Gabriel Stokes on water wave theory. *Annual Reviews of Fluid Mechanics*, 37, pp.23-42.
- Dewar, W.K., 1980. The Effect of Internal Waves on Neutrally Buoyant Floats and Other Near-Lagrangian Tracers. M.S. Thesis, MIT, 78 pages.
- Franks, P.J.S., 1997. Spatial patterns in dense algal blooms. *Limnology and Oceanography*, 42(5 part 2), pp.1297–1305.
- Gaines, S. & Roughgarden, J., 1985. Larval settlement rate: A leading determinant of structure in an ecological community of the marine intertidal zone. *Proceedings of the National Academy of Sciences of the United States of America*, 82(11), pp.3707–11.
- Henderson, S.M. 2016. Upslope internal-wave Stokes drift, and compensating downslope Eulerian mean currents, observed above a lakebed. *Journal of Physical Oceanography* 46, pp.1947-1961.
- Inall, M.E., Shapiro, G.I. & Sherwin, T.J., 2001. Mass transport by non-linear internal waves on the Mali Shelf. *Continental Shelf Research* 21, pp. 1449-1472.
- Jaffe, J.S. et al., 2017. A swarm of autonomous miniature underwater robot drifters for exploring submesoscale ocean dynamics. *Nature Communications*, 8:14189, doi:10.1038/ncomms14189.
- Kamykowski, D., 1974. Possible interactions between phytoplankton and semidiurnal internal tides. *Journal of Marine Research*, 32, pp.67-89.
- Kumar, N. et al., 2015. Midshelf to Surfzone Coupled ROMS–SWAN model data comparison of waves, currents, and temperature: diagnosis of subtidal forcings and response. *Journal of Physical Oceanography*, 45(6), pp.1464–1490.
- Lamb, K.G., 1997. Particle transport by nonbreaking, solitary internal waves. *Journal of Geophysical Research: Oceans*, 102(C8), pp.18641–18660.
- Lennert-Cody, C.E. & Franks, P.J.S., 2002. Fluorescence patches in high frequency internal waves. *Marine Ecology Progress Series*, 235, pp.29–42.
- Lennert-Cody, C.E. & Franks, P.J.S., 1999. Plankton patchiness in high-frequency internal waves. *Marine Ecology Progress Series*, 186, pp.59–66.

647 Lucas, A.J., P.J.S. Franks & C.L. Dupont. 2011. Horizontal internal-tide fluxes support  
648 elevated phytoplankton productivity over the inner continental shelf. *Limnology and*  
649 *Oceanography: Fluids and Environments*, 1, 10.1215/21573698-1258185.  
650

651 Omand, M.M., J.J. Leichter, P.J.S. Franks, R.T. Guza, A.J. Lucas & F. Feddersen. 2011.  
652 Physical and biological processes underlying the sudden surface appearance of a red  
653 tide in the nearshore. *Limnology and Oceanography*, 56(3), pp.787-801.  
654

655 Ou, H.W. & L. Maas. 1986. Tidal-induced buoyancy flux and mean transverse  
656 circulation. *Continental Shelf Research* 5(6), pp.611-628.  
657

658 Pineda, J., 1999. Circulation and larval distribution in internal tidal bore warm fronts.  
659 *Limnology and Oceanography*, 44(6), pp.1400–1414.  
660

661 Rosenfeld, L.K. & Beardsley, R.C., 1987. Barotropic semidiurnal tidal currents off  
662 northern California during the coastal ocean dynamics experiment (CODE). *Journal*  
663 *of Geophysical Research*, 92(C2), pp.1721–1732.  
664

665 Scotti, A. & Pineda, J., 2007. Plankton accumulation and transport in propagating  
666 nonlinear internal fronts. *Journal of Marine Research*, 65(1), pp.117–145.  
667

668 Shanks, A. L., 1983. Surface slicks associated with tidally forced internal waves may  
669 transport pelagic larvae of benthic invertebrates and fishes shoreward. *Marine*  
670 *Ecology Progress Series*, 13, pp.311–315.  
671

672 Shanks, A.L., 2009. Pelagic larval duration and dispersal distance revisited. *Biological*  
673 *Bulletin*, 216(3), pp.373-385.  
674

675 Shanks, A.L. and L. Brink. 2005. Upwelling, downwelling, and cross-shelf transport of  
676 bivalve larvae: test of a hypothesis. *Marine Ecology Progress Series* 302, pp.1-12.  
677

678 Shanks, A.L. et al., 2014. Onshore transport of plankton by internal tides and upwelling-  
679 relaxation events. *Marine Ecology Progress Series*, 502, pp.39–51.  
680

681 Shanks, A.L., J. Largier, L. Brink, J. Brubaker & R. Hoof. 2000. Demonstration of the  
682 onshore transport of larval invertebrates by the shoreward movement of an upwelling  
683 front. *Limnology and Oceanography*, 45(1), pp.230-236.  
684

685 Shanks, A. L. & G. Wright, W., 1987. Internal-wave-mediated shoreward transport of  
686 cyprids, megalopae, and gammarids and correlated longshore differences in the  
687 settling rate of intertidal barnacles. *Journal of Experimental Marine Biology and*  
688 *Ecology*, 114(1), pp.1–13.  
689

690 Shroyer, E.L., Moum, J.N. & Nash, J.D., 2010. Vertical heat flux and lateral mass  
691 transport in nonlinear internal waves. *Geophysical Research Letters*, 37, L08601,  
692 doi:10.1029/2010GL042715

693  
694 Thorpe, S. A., 1968. On the Shape of Progressive Internal Waves. Philosophical  
695 Transactions of the Royal Society A: Mathematical, Physical and Engineering  
696 Sciences, 263(1145), pp.563–614.  
697  
698 Wunsch, C. 1971. Note on some Reynolds stress effects of internal waves on slopes.  
699 Deep-Sea Research 18, pp.583-591.  
700  
701 Zhang, S., Alford, M.H. & Mickett, J.B., 2015. Characteristics, generation and mass  
702 transport of nonlinear internal waves on the Washington continental shelf. Journal of  
703 Geophysical Research – Oceans, 120(2), pp.741-758.



Table 1. Stream functions and Stokes velocities for neutrally buoyant organisms, and depth-keeping organisms in linear internal waves of general form, with linear stratification, and waters with a pycnocline.

Case	Stream function $\psi(x,z)$	Neutrally buoyant Stokes velocity $u_{Snb}$	Depth-keeping Stokes velocity $u_{Sd-k}$
General	$A_{\max} \frac{\omega}{k} S_w(z) \cos(kx - \omega t)$	$\frac{A_{\max}^2 \omega}{2k} \left[ \left( \frac{dS_w(z)}{dz} \right)^2 + S_w(z) \frac{d^2 S_w(z)}{dz^2} \right]$	$\frac{A_{\max}^2 \omega}{2k} \left( \frac{\partial S_w(z)}{\partial z} \right)^2$
Linear stratification	$A_{\max} \frac{\omega}{k} \sin \frac{\pi z}{H} \cos(kx - \omega t)$	$\frac{A_{\max}^2 \pi^2 \omega}{2kH^2} \cos \left( \frac{2\pi z}{H} \right)$	$\frac{A_{\max}^2 \omega \pi^2}{2kH^2} \cos^2 \left( \frac{\pi z}{H} \right)$
Pycnocline	$A_{\max} \frac{\omega}{k} \operatorname{sech}^{kz_{scale}} \left( \frac{z - z_{pyc}}{z_{scale}} \right) \cos(kx - \omega t)$	$\frac{A_{\max}^2 \omega}{2} \operatorname{sech}^{2kz_{scale}} \left( \frac{z - z_{pyc}}{z_{scale}} \right) \cdot \left[ 2k - \left( \frac{1}{z_{scale}} + 2k \right) \operatorname{sech}^2 \left( \frac{z - z_{pyc}}{z_{scale}} \right) \right]$	$\frac{A_{\max}^2 \omega k}{2} \operatorname{sech}^{2kz_{scale}} \left( \frac{z - z_{pyc}}{z_{scale}} \right) \tanh^2 \left( \frac{z - z_{pyc}}{z_{scale}} \right)$

## Figure Captions

Figure 1. Stokes velocity in linear internal waves. (a,e) Density profile, (b,f) structure of the vertical velocity  $S_w(z)$ , (c,g) vertical displacement of evenly spaced tracer lines (wave is propagating to the right, as shown by the arrow), (d,h) vertical profile of the Stokes velocity of neutrally buoyant organisms (dashed line) and depth-keeping organisms (solid line). Negative values indicate velocity to the left, positive to the right (in the direction of wave propagation). (a-d) Linear stratification, (e-h) analytical pycnocline.

Figure 2. Comparison of numerical and analytical Stokes velocities. Stokes velocities for neutrally buoyant (solid line from model, dashed from equations 7 and 10) and depth-keeping (solid with circles from model, dotted from equations 9 and 10) organisms in the linear stratification of figure 1. Positive values show transport in the direction of the wave's phase. Agreement is such that numerical and analytical results are almost completely superimposed.

Figure 3. Power spectrum of the first EOF of vertical velocity. The high-frequency internal waves have periods of 20-30 minutes. Thin vertical line shows the 25-minute period used for the Stokes velocity calculations of figure 4.

Figure 4. Stokes velocities calculated from in situ data. (a,d,g) Temperature profiles at the beginning, middle, and end of a 12.42 hour M2 tidal period. (b,e,h) First EOF of vertical velocities ( $S_w(z)$ , circles), and the polynomial fit to the data (solid line). (c,f,i) Stokes velocities calculated from the EOFs for neutrally buoyant organisms (dashed lines, equation 7), and depth-keeping organisms (solid lines, equation 9). Positive velocities are in the direction of the phase propagation of the wave.

Figure 5. Stokes velocities associated with a range of swimming abilities. Maximum swimming velocities for various particles are represented as a fraction of the maximum wave vertical velocity ( $w_{max} = 0.0027 \text{ m s}^{-1}$ ). Stratification and wave properties are the same as for figure 2. Positive values show transport in the direction of the wave's phase.

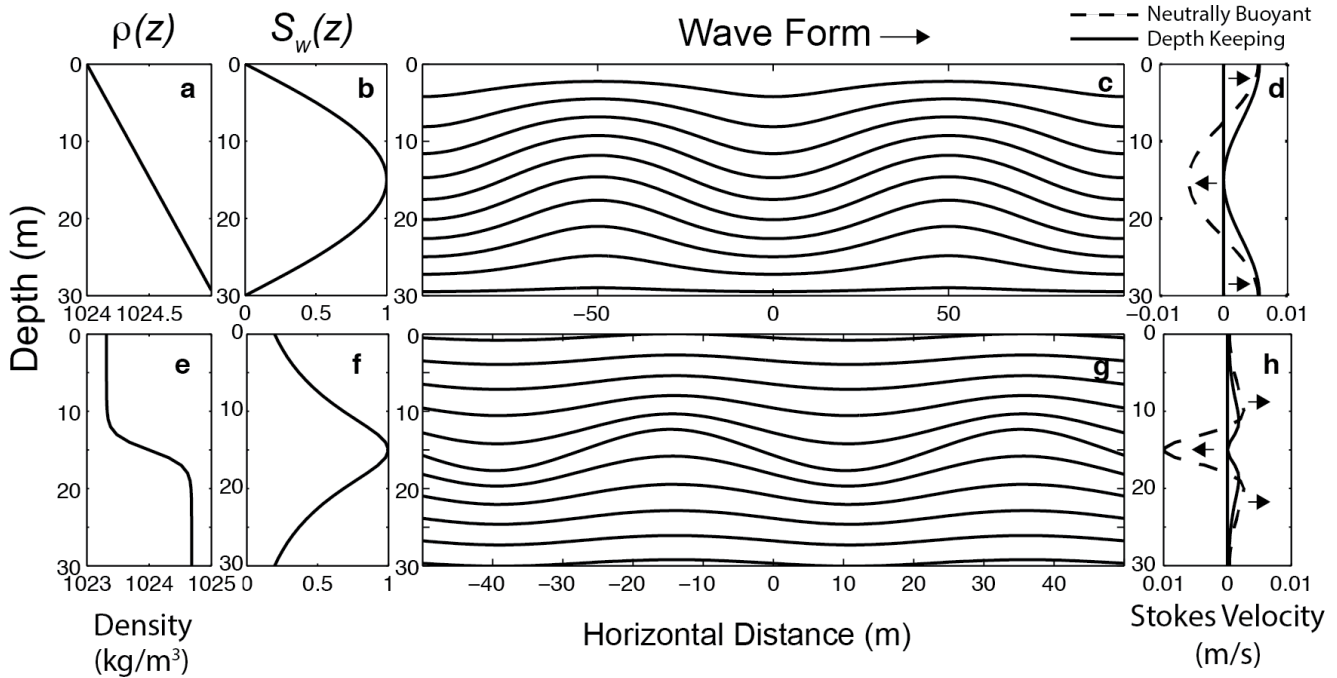


Figure 1. Stokes velocity in linear internal waves. (a,e) Density profile, (b,f) structure of the vertical velocity  $S_w(z)$ , (c,g) vertical displacement of evenly spaced tracer lines (wave is propagating to the right, as shown by the arrow), (d,h) vertical profile of the Stokes velocity of neutrally buoyant organisms (dashed line) and depth-keeping organisms (solid line). Negative values indicate velocity to the left, positive to the right (in the direction of wave propagation). (a-d) Linear stratification, (e-h) analytical pycnocline.

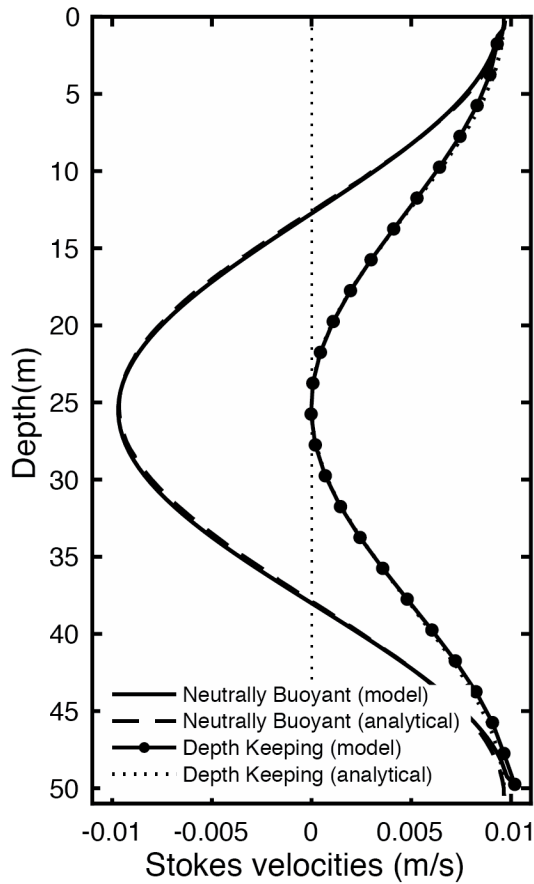


Figure 2. Comparison of numerical and analytical Stokes velocities. Stokes velocities for neutrally buoyant (solid line from model, dashed from equations 7 and 10) and depth-keeping (solid with circles from model, dotted from equations 9 and 10) organisms in the linear stratification of figure 1. Positive values show transport in the direction of the wave's phase. Agreement is such that numerical and analytical results are almost completely superimposed.

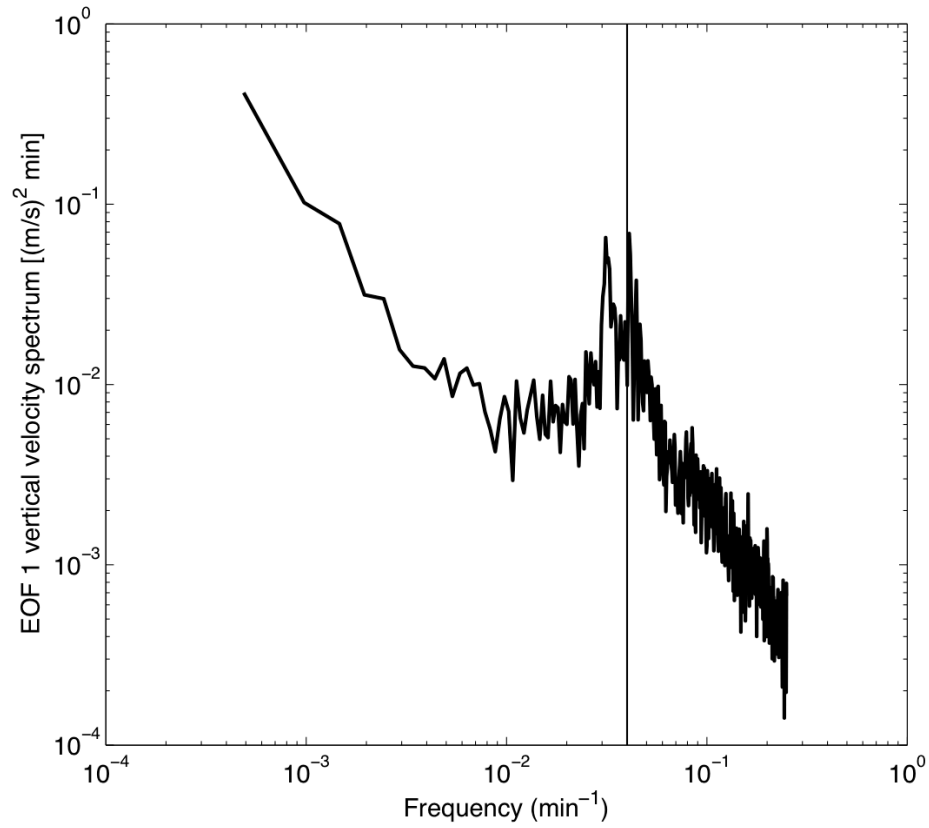


Figure 3. Power spectrum of the first EOF of vertical velocity. The high-frequency internal waves have periods of 20-30 minutes. Thin vertical line shows the 25-minute period used for the Stokes velocity calculations of figure 4.

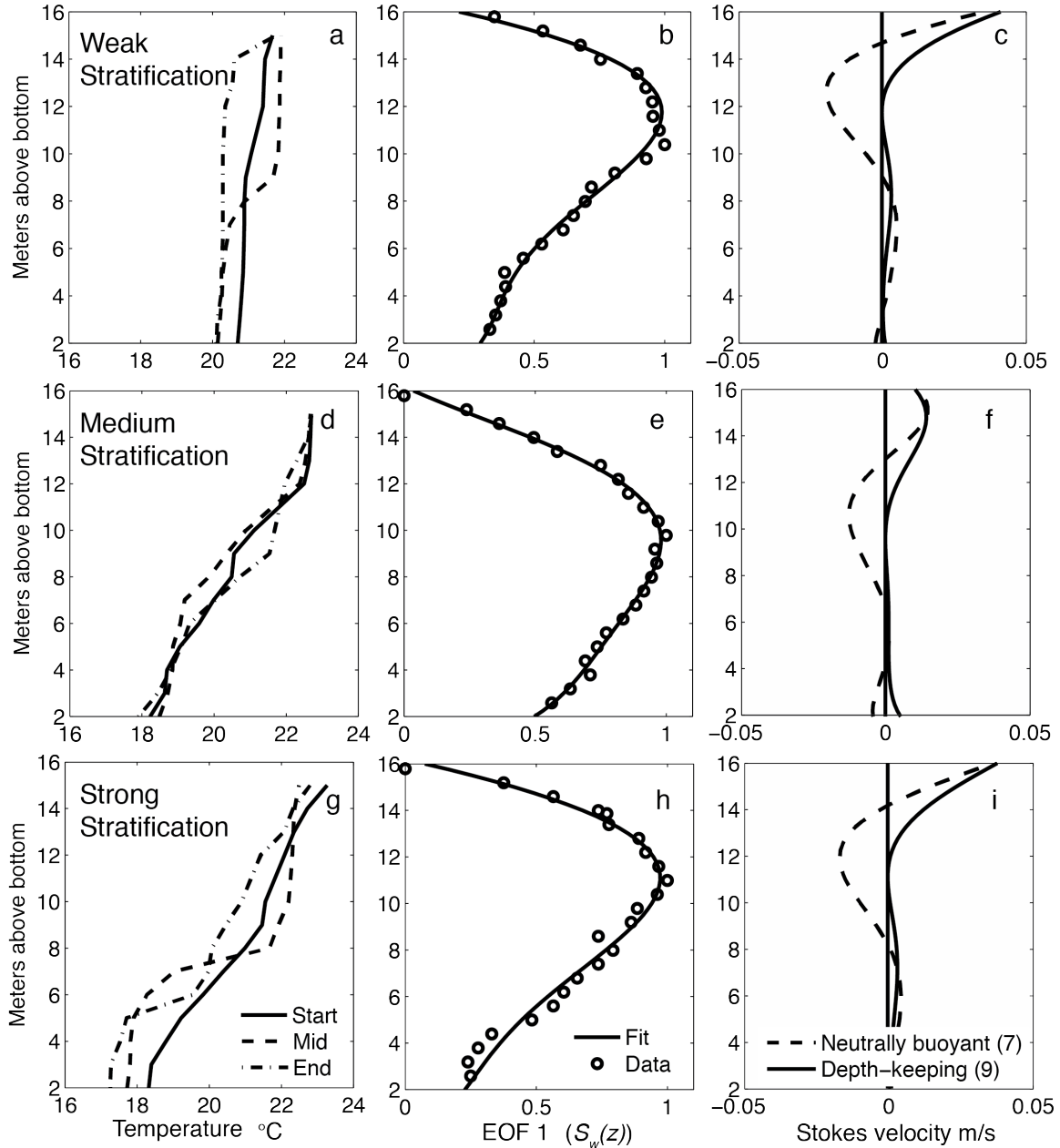


Figure 4. Stokes velocities calculated from *in situ* data. (a,d,g) Temperature profiles at the beginning, middle, and end of a 12.42 hour M2 tidal period. (b,e,h) First EOF of vertical velocities ( $S_w(z)$ , circles), and the polynomial fit to the data (solid line). (c,f,i) Stokes velocities calculated from the EOFs for neutrally buoyant organisms (dashed lines, equation 7), and depth-keeping organisms (solid lines, equation 9). Positive velocities are in the direction of the phase propagation of the wave.

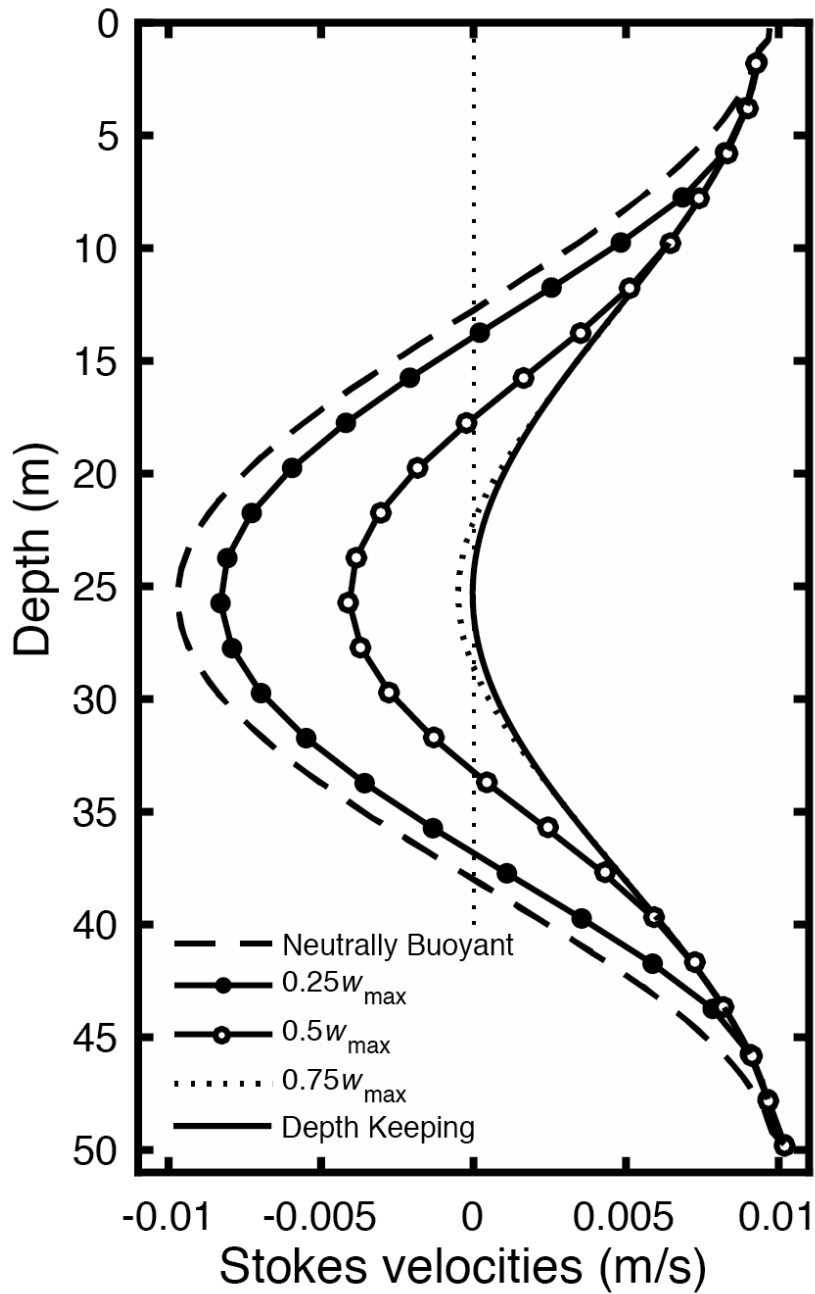


Figure 5. Stokes velocities associated with a range of swimming abilities. Maximum swimming velocities for various particles are represented as a fraction of the maximum wave vertical velocity ( $w_{\max} = 0.0027 \text{ m s}^{-1}$ ). Stratification and wave properties are the same as for figure 2. Positive values show transport in the direction of the wave's phase.